A SCUBA survey of compact dark Lynds clouds.

A.E. Visser, J.S. Richer, and C.J. Chandler[1]

ABSTRACT

We present the first results of a submillimetre continuum survey of Lynds dark clouds. Submillimetre surveys of star forming regions are an important tool to obtain representative samples of the very first phases of star formation. Maps of 24 small clouds were obtained with SCUBA, the bolometer array receiver at the James Clark Maxwell Telescope, and 19 clouds were detected. The total dark cloud area surveyed was $\sim$130 arcmin^2, and a total gas mass of 90 $M_\odot$ was detected. The dust emission is in general in good agreement with the extinction of optical starlight. The observed clouds contain a newly discovered protostar in L944, and a previously known protostar IRAS 23228+4320 in L1246. Another 8 starless cores, either gravitationally unbound, or pre-stellar in nature, have also been detected. All starless cores and protostars are detected in only 7 clouds, and the remaining 17 clouds seem quiescent and do not show any signs of recent star formation activity. The 850-μm images of all detected clouds are presented as well as 450-μm images of L328, L944, L1014, and L1262. The outflows of the protostars in L944 and L1246 have also been discovered and are mapped in ^{12}CO $J = 2 \rightarrow 1$. The detection of the young protostar in L944, which is not present in the IRAS point source catalogue, shows the capacity of submillimetre surveys to detect unknown protostars.

Subject headings: stars: formation - ISM: clouds - ISM: dust, extinction - ISM: jets and outflows

---

[1]Postal address: Cavendish Astrophysics, Cavendish Laboratory, Madingley Road, Cambridge CB3 0HE, United Kingdom

1. Introduction

Protostars are thought to evolve from pre-stellar cores to Class 0, I, II and III objects successively (André et al. 1999). A pre-stellar core is a gravitationally bound object in a molecular cloud, which does not yet contain a central hydrostatic protostar. This core evolves towards higher degrees of central condensation and will collapse when the pressure forces are no longer capable of holding the material against gravity. There are different theories of what the initial conditions for collapse might be and how the collapse phase proceeds. Shu (1977) uses a singular isothermal sphere to describe the density distribution in a pre-stellar core on the verge of collapse ($\rho = a^2/2\pi G r^2$ where a is the isothermal sound speed). The cloud collapse begins at the center of the cloud and material will accrete onto the central condensation at a constant rate, $\dot{M}_{acc} \approx a^3/G$. Foster & Chevalier (1993), however, take a Bonnor-Ebert sphere as the initial condition for collapse, predicting a mass accretion rate which *decreases* with time. A Bonnor-Ebert sphere is also isothermal but has a flattened central density initially, and by the time an r^{-2} density profile is established the gas is flowing inwards supersonically. Another difference is that the Bonner-Ebert sphere as used by Foster & Chevalier is bounded while a singular isothermal sphere is not. Isothermal axisymmetric models of core evolution that take ambipolar diffusion and magnetic fields into account are proposed by Ciolek & Mouschovias (1994), and Basu & Mouschovias (1995). These models also predict pre-stellar cores with flat inner density profiles. The isothermal equation of state is a sensible first approximation for interstellar clouds, but the assumption that the gas remains isothermal throughout collapse might not be true. Theoretical models of star formation in non-isothermal spheres predict a variety of collapse histories and accretion rates. McLaughlin & Pudritz (1997) for instance, find that the core accretion rate in a sphere with a logotropic equation of state *increases* with time.

The youngest protostars are Class 0 sources, young stellar objects which still need to accrete most of their mass from the surrounding envelope ($M_{env} > M_*$). Characteristics of these sources are very strong submillimetre continuum emission, no detectable emission at wavelengths shorter than $\sim 10\,\mu$m, a spectral energy distribution resembling that of a single temperature black body

(T $\leq$ 30 K), and the presence of a molecular outflow (André et al. 1993). The initial epoch of vigorous accretion predicted by the models of Foster & Chevalier (1993) might correspond to the Class 0 phase (see also Henriksen et al. 1997). After this initial high accretion phase, the accretion rate settles down to values similar to rates predicted by Shu's models, before it declines again at later times due to the finite reservoir of mass. This phase of late accretion might correspond to the Class I phase. Class I sources are visible in the infrared and their spectral energy distribution is broader than a single-temperature blackbody. The envelopes of young stellar objects will be mostly cleared away after the Class I phase, and protostars become optically visible. The protostar is now a classical T Tauri star and has an optically thick disk (Class II object, CTTS) and evolves into a weak-line T Tauri star (Class III object, WTTS), with an optically thin disk (Lada & Wilking 1984).

Class I, II and III sources are called infrared protostars and samples of these more evolved objects are believed to be essentially complete due to surveys made with the Infrared Astronomical Satellite IRAS (e.g. Kenyon et al. 1990) and infrared telescopes at 2 μm (Gomez et al. 1994). The relative statistical lifetimes of these phases are therefore well established. Absolute lifetimes for T Tauri stars (Class II and III) are based on pre-main sequence HR diagram tracks (e.g. Cohen & Kuhi 1979) and vary from a few times 10^5 yr up to a few times 10^7 yr. Usually an estimated age of 10^6 yr is adopted for CTTS and 10^7 yr for WTTS (Kenyon & Hartmann 1990). The lifetime of (1-2) $\times$ 10^5 yr for Class I objects is obtained from the ratio of the Class I sources relative to T Tauri stars (Kenyon et al. 1990; Wilking et al. 1989). The lifetimes of Class 0 sources are not very well constrained. Class 0 sources are not visible at wavelengths shorter than $\sim$ 10 μm and since many of these objects were found serendipitously, complete samples do not exist. The estimated lifetime of 10^4 yr is based on the small number of Class 0 sources relative to the Class I sources identified in the ρ Ophiuchi cloud (André & Montmerle 1994; Motte et al. 1998). It is clear that to verify the different low-mass star formation theories, complete samples of pre-stellar cores and protostars in all phases are needed. With a sample of pre-stellar cores the initial collapse conditions can be studied (Ward-Thompson et al. 1994; André et al. 1996). With a complete sample of Class 0 objects the statistical lifetime of this phase can be established, which will constrain the mass accretion rate.

To obtain complete samples of pre-stellar cores and protostars (Class 0 and Class I sources) we have commenced a submillimetre survey of dark molecular clouds, the birthsites of low-mass stars. A survey of dark molecular clouds at submillimetre wavelengths is for the first time possible in a reasonable amount of time due to the new array receivers such as the Submillimetre Common-User Bolometer Array (SCUBA) on the James Clerk Maxwell Telecope (JCMT), the instrument used for this survey. The compact submillimetre cores identified in the mapped clouds are either protostars or starless cores, and to decide their nature the submillimetre survey was followed by a limited ^{12}CO $J = 2 \rightarrow 1$ survey to search for outflow activity, indicative of an embedded protostar.

The dark molecular clouds observed are all Lynds class 6 clouds. The Lynds dark nebulae catalogue contains 1802 optically selected dark clouds from the POSS plates (Lynds 1962), of which 147 clouds are classified as class 6. Estimates of the opacity of the Lynds clouds were made on a scale of 1 to 6, with the class 6 clouds being the most opaque ($A_V \gtrsim 5$ mag, Lynds 1962). These visual estimates were based on a comparison of the cloud with the neighbouring fields for the particular Palomar photograph on which the cloud appeared, and the classification is therefore somewhat subjective. By observing an optically selected sample of molecular clouds, avoiding any selection based on the infrared and IRAS properties, we hope to establish in an unbiased way the star forming properties of the local molecular clouds. In addition, this survey also provides a homogeneous sample to study the structure of the clouds and the outflow phenomenon. In this paper we present the “jiggle” maps of a sample of small clouds (minor axis smaller than 2.2 arcminutes). In a future paper scan maps of a sample of larger clouds will be presented.

2. Observations and data reduction

2.1. Submillimetre continuum images

Jiggle maps of 24 Lynds class 6 clouds were obtained in 1997 September using SCUBA at the JCMT on Mauna Kea, Hawaii. SCUBA was built by the Royal Observatory Edinburgh and is the most versatile and sensitive of a new generation of submillimetre cameras (Holland et al. 1998). SCUBA has two arrays of bolometric detectors which can be used simultaneously by means of a dichroic beamsplitter. The arrays are cooled to a temperature of 0.1 K to achieve high sensitivity. We used the short-wavelength array at 450 μm and the long-wavelength array at 850 μm, for which the arrays are optimised. The arrangement of the bolometers is such that the sky is instantaneously under-sampled, and for simultaneous dual wavelength imaging a 64 point jiggle pattern with 3 arcsec sampling is needed which is achieved by moving the secondary mirror (Holland et al. 1998). This 64 jiggle pattern was repeated four times, with offsets of $\pm$ 12 arcsec in both R.A. and Dec. to eliminate holes in the maps caused by a small number of noisy bolometers, and to improve the signal-to-noise ratio. The secondary mirror chopped to an off-source reference position with a chop throw of $150''$, the chop direction being dependent on the morphology of the cloud. Skydip observations were carried out regularly and the atmospheric opacity was found to be stable, although the atmosphere became steadily more opaque during the 6 nights of the observing run. The atmospheric zenith opacity varied from 0.26 (first night) to 0.59 (last night) at 850 μm, conditions not good enough to obtain 450-μm images. The pointing accuracy was checked frequently using Mars, Uranus, and other pointing sources close to the Lynds clouds. Pointing corrections were generally small (typically 2-3 arcsec). The data were calibrated against Mars and Uranus, for which jiggle maps were obtained with the same chop throw used for the Lynds clouds. The uncertainty in the calibration is $\sim$20% at 850 μm, and $\sim$50% at 450 μm due to fluctuations in the optical depth of the atmosphere, and from uncertainties in the coupling efficiency of the beam to the calibrators.

Both arrays have a field-of-view of approximately 2.3 arcminutes in diameter, and the clouds observed were therefore selected to have a semi-minor axis smaller or equal to 1.1 arcmin, as measured by Parker (1988). If an elongated cloud did not fit in one SCUBA field of view the final map of the object was obtained by mosaicing adjacent jiggle maps. All clouds in this sample are thus compact in at least one dimension. In Table 1 the Lynds names are presented of the clouds observed. Also in Table 1 are names for the clouds from the Barnard (B) catalogue (1927) and the Clemens and Barvainis (CB) catalogue (1988). Of the 147 Lynds class 6 clouds, 66 have a semi-minor axis smaller or equal to 1.1 arcmin. The selection of the 24 clouds observed from these 66 was based on R.A. and Dec. at the time of observing. The sample of clouds was thus essentially chosen in a random fashion and should provide a representative selection of these small, optically identified Lynds class 6 clouds.

The most striking dense cores (L328, L944, L1014 and L1246) were observed again in 1998 July, under better weather conditions ($\tau_{225\,\mathrm{GHz}} \leq 0.04$) to obtain the 450 μm flux densities. These cores have a high flux density ($>$ 140 mJy/beam at 850 μm) and are centrally condensed. Uranus was used for the flux calibration. The chop throw was $120''$ and again pointing accuracy was checked regularly. Skydips were performed to obtain the zenith opacities, which were stable with values τ_{450} = 0.56 and τ_{850} = 0.12. Because both wavelengths are observed at the same time, we also obtained more 850-μm data which were added to the previously-obtained data. The 850-μm beamsize is $\sim 15''$ and the 450-μm beamsize is $\sim 8''$.

Data reduction was performed using the SCUBA User Reduction Facility, SURF (Jenness & Lightfoot 1998). The maps were flatfielded, and then corrected for the atmospheric extinction using skydip measurements before and after the observation. The sky noise was removed using the SURF task ‘remsky’, for which we carefully selected bolometers in the array which did not detect source emission. Spikes and noisy bolometer measurements were removed from the data, and the data were rebinned into equatorial coordinates using a linear weighting function.

2.2. ^{12}CO $J = 2 \rightarrow 1$ observations

To search for outflows from the submillimetre cores we made a fivepoint pattern of ^{12}CO $J = 2 \rightarrow 1$ (230.538 GHz) spectra with the middle spectrum on the dust peak from the SCUBA 850-μm map. The observations were carried out in 1998 July, using receiver A2 at the JCMT. The system temperature was typically 440 K and the integration time of each spectrum was 2 minutes, achieving a noise level of 0.2 K in a bandwidth of 0.16 MHz (resolution is 0.2 km/s). Two of the cores were found to have high velocity gas and maps of their outflows were made using the raster mapping mode with a cell size of $5''$ and an integration time of 5 seconds per point. The spectra were taken by position-switching to eliminate instrumental and atmospheric effects. Pointing was checked regularly and the system was calibrated using standard chopper wheel techniques to obtain spectra on the T_A^* scale. When deriving the masses and flow energetics from the spectra, we assumed a main beam efficiency of 0.66.

3. Results of submillimetre continuum imaging

3.1. Maps

The 24 clouds observed are listed in Table 1, with positions adopted from Parker (1988). The total area surveyed is 320 arcmin^2, generously covering the dark clouds (see Figure 1, where the dashed line indicates the observed area). The clouds can be approximated by ellipses and by using the sizes of these ellipses the total area of dark cloud covered can be estimated. Parker (1988) uses parameter E to indicate how closely an ellipse may be fitted to each cloud ($E = A_{in}/A_{tot}$, where A_{in} is the area of the cloud lying within the ellipse and A_{tot} the total area of the cloud). The clouds in this sample have typically E = 0.75, and the total area of dark cloud observed becomes 130 arcmin^2.

Of the 24 clouds observed, 5 were undetected (L53, L226, L229, L231, and L233), which is 20% of the sample. The noise levels on these jiggle maps vary from 23 to 37 mJy/$14''$ beam on each 3″ pixels (see Table 2), and the 1σ contours show structure consistent with noise. When the images of the undetected clouds are smoothed, some structure can be seen. These features are however equally negative and positive and do not correlate with the optical appearances of the clouds. Some 3σ features occur on the edges of the smoothed maps but are the result of the rebinning into equatorial coordinates and are not real detections. We conclude that these 5 clouds are not detected at our sensitivity level.

The extended dust emission from the 19 detected clouds correlates sometimes very well with the optical appearances of the clouds on the STScI Digitized Sky Survey images[2], see for instance L31, L860, L951 and L953. The images of the four clouds observed at both 450 μm and 850 μm are presented in Figure 1a. We present the 850-μm images of the remaining detected Lynds clouds in Figure 1b. All the images are smoothed with a small gaussian (FWHM varying from 14″ to 24″), which greatly improves the signal-to-noise ratio on the maps, and allows faint extended structure to be seen.

In Table 2 we present the 850-μm peak flux densities and integrated flux densities of the detected clouds, as measured on the unsmoothed maps. The integrated flux densities were obtained by integrating the flux density within a box around the extended emission of the cloud. The peak flux densities and integrated fluxes at 450 μm are also presented in Table 2 for the relevant clouds.

3.2. Masses and densities

3.2.1. Masses

The correct distances towards the clouds need to be known to be able to derive meaningful physical parameters from the data. In Table 1 the assumed distances are listed and in the appendix

---

[2]The Digitized Sky Surveys were produced at the Space Telescope Science Institute under U.S. Government grant NAG W-2166 (see http://stdatu.stsci.edu/dss/acknowledgement.html).

it is explained how these were obtained. The masses of the clouds and cores can be estimated via $M = F_\nu D^2/\kappa_\nu B_\nu(T_{\rm dust})$, where F_ν is the flux density, D the distance towards the cloud, $B_\nu(T)$ the Planck function for temperature $T_{\rm dust}$, and κ_ν the dust opacity. The assumption has been made that the dust emission is optically thin, a condition satisfied in most molecular clouds. Only in the densest environments such as in protostellar discs will the dust become optically thick at shorter wavelengths ($\tau_{450\mu{\rm m}} \gtrsim 1$ for $A_\nu \gtrsim 8000$ mag). The important variables in calculating the masses from the thermal dust emission are the dust temperature and the dust opacity. We assumed here a dust temperature of 12 K realising that although this is a sensible temperature for quiescent dark molecular clouds, it might be an underestimate for the temperature in dark clouds containing young stellar objects, such as L1246. The dust temperature in dark clouds such as these are measured to be in between 10 and 15 K (Myers & Benson, 1983). More recently, typical dust temperatures in star forming cores have been established to be $\sim$12 K (Williams, 1999; Bacmann, 2000). An assumed temperature of 12 K seems therefore appropriate for these calculations, however, if the dust is as cold as 10 K the masses are underestimated with $\sim$40%, and similar, if the dust is 15 K, the masses are overestimated with $\sim$35%. The dust opacity is often parameterized as a power-law function of frequency at long wavelengths, $\kappa_\nu = \kappa_0(\nu/\nu_0)^\beta$. Different values of κ_ν can be found in the literature (Henning et al. 1995), and we adopt here the value $\kappa_{850\mu m} = 0.001\,{\rm m^2\,kg^{-1}}$, using the Hildebrand (1983) assumptions, with $\beta = 2$. This estimate of $\kappa_{850\mu m}$ should be correct within a factor of 3. The distances in Table 1 are used and the calculated peak masses and cloud masses are presented in Table 3. The total mass traced by the dust is $90\,M_\odot$, of which $40\,M_\odot$ is present in L1246. Note, however, that the calculated mass is proportional to the uncertain distance squared, and L1246 is the most distant cloud. A temperature of 12 K is also likely to be an underestimate for a cloud containing a protostar and a higher temperature would decrease the calculated mass.

3.2.2. Column and space densities

The peak H_2 column densities have been calculated assuming again a dust temperature of 12 K and an 850-μm dust opacity of 0.001 m^2kg^{-1}. Corresponding peak extinction ($N(H_2) = A_v \times 0.95 \times 10^{25}\,m^{-2}$; Bohlin et al. 1978) and peak space densities have been derived from the peak column densities and all are presented in Table 3. We have assumed that the depth of the cloud is similar to the beamsize at the distance towards the cloud when calculating the space density. Although this is an objective way to calculate space densities, it is likely to be an overestimate. The material is probably distributed in a volume typically 3-4 times larger (the typical size of a core where the peak emission is measured is a few beamwidths across as can be seen in the Figures). The cloud column densities are also presented in Table 3. The mean cloud column density is $5 \times 10^{25}\,m^{-2}$ corresponding to A_v = 5 mag, as expected for dark clouds such as these. The extinction where the dust emission peaks is of course higher, and A_v varies from 8 to 56 mag. The average peak column density is $1.6 \times 10^{26}\,m^{-2}$. Naturally, all these values are just indications due to the uncertainties in the dust temperature, dust opacity and calibration conversion factor. The noise levels on the maps of the undetected clouds are on average slightly higher than the noise levels on the detected maps, and it is very likely that we just missed the sensitivity to detect these clouds. The upper levels presented in Table 3 for these clouds are also only valid when the dust temperature is 12 K, and the dust opacity is 0.001 m^2kg^{-1}. It is of course possible that more gas is present in these undetected clouds if the dust temperature is lower than 12 K, especially since the Planck function is strongly dependent on the temperature at these wavelengths and low temperatures.

4. Submillimetre cores

4.1. Identification of cores and IRAS associations

The purpose of this survey is to identify samples of pre-stellar cores and protostars (Class 0 and Class I sources). In order to obtain a list of compact objects we spatially filtered the images by smoothing each SCUBA map with a 2 arcminutes gaussian, and subtracting the smoothed map from the original image. The remaining image contains only compact structures, and all $\geq 3\sigma$ structures were identified as candidate submillimetre cores. Four such cores (in L31, L55 and two in L917) were rejected since they appear near the edge of the map where spiky negative and positive features can occur. The remaining 10 submillimetre cores (SMM), their positions (accurate within 3-4 arcsec) and peak flux densities are listed in Table 4. A 3σ detection could potentially be just noise, but in the Figures it can be seen that the 10 cores look like real dust condensations embedded in the clouds. These cores are either protostars or starless, and more observations are needed to determine their nature.

More evolved protostars are usually associated with IRAS sources. Of the 24 Lynds clouds 7 are associated with an IRAS source (Parker, 1988, Launhardt & Henning, 1997), and in Table 2 the IRAS associations are listed. The IRAS colours of 16482−1906 (L31), 17375−1936 (L226) and 19116+1623 (L709) suggest that these sources are either field stars (characterized by a flux ratio $F_\nu(12\mu\mathrm{m})/F_\nu(25\mu\mathrm{m})\sim$2-4, Kenyon et al. 1990) or T Tauri stars (detected at 12 μm and not at 100 μm with their spectral energy distributions (SEDs) rising towards shorter wavelengths). Field stars and T Tauri stars are not expected to be detected at 850 μm, and we do indeed not see these IRAS sources in the SCUBA maps. The colours of IRAS 17205−2359 (L53) suggest this source could be a very young protostar (Class 0) since it is detected at 100 μm, the SED is steeply rising from 60 μm to 100 μm, and no emission short-ward of 60 μm has been detected. We detect no emission at 850 μm however, and the presence of a prestellar core or young protostar is unlikely. The HIRES-processed[3] image of this IRAS source shows an extended source at 60 μm,

[3] We requested HIRES images of some of the dark clouds via electronic mail to IPAC. The Infrared Processing and Analysis Center (IPAC)

and we conclude that the FIR emission is caused by cirrus. Cirrus is usually detected at just 100 μm or at both 60 and 100 μm with $\log(F_\nu(100\mu\mathrm{m})/F_\nu(60\mu\mathrm{m})) > 0.6$, and is too cold to be detected at 25 μm (Emerson, 1987). The non-detection of this cirrus cloud at 850 μm suggests that it is cold ($T \leq 20$ K) with a high value for the frequency dependence of the dust opacity ($\beta \geq 2$). Submillimetre observations of a cirrus cloud in the Polaris Flare were also found to be consistent with emission from cold dust (T = 13 K) with a steep dust emissivity index of $\beta = 2.2$ (Bernard et al. 1999). Huard et al. (1999) mapped 15 cold IRAS sources associated with Bok globules using SCUBA. Although these IRAS sources are strong 100 μm emitters, 9 of them have not been detected at submillimetre wavelengths. Huard et al. also conclude that the infrared emission of these non-detections is cirrus emission. IRAS 21186+4320 (L951) might also be cirrus, but although the position from the IRAS point source catalogue (PSC) is covered by our 850 μm map, the 100-μm peak emission on a HIRES-processed IRAS map seems to be north east of the PSC position, on the edge of the SCUBA map of L951. The final IRAS source associated with L1246, IRAS 23228+6320, has the colours of a protostar.

4.2. Classifying the cores

Of the 10 submillimetre cores only one can be identified with a known protostar (L1246−SMM1) through its association with an IRAS source. The nature of the other cores can not be determined from the SCUBA images alone, and a limited ^{12}CO survey has been carried out to search for outflow activity. All protostars are thought to drive outflows and the accretion process onto the protostar is probably physically linked to the outflow process (Königl & Pudritz 1999). Pre-stellar cores do not drive outflows and the presence of an outflow might therefore suggest that the submillimetre core contains an embedded protostar. For this reason we searched for outflows of all cores (apart from L860−SMM1 and L860−SMM2, due to limited observing time) in ^{12}CO

---

is funded by NASA as part of the IRAS extended mission under contract to the Jet Propulsion Laboratory (JPL). The HIRES image construction algorithm uses the maximum correlation method to iteratively construct resolution-enhanced images (Aumann et al. 1990). Most of the spatial information is obtained in the first iterations and we have therefore chosen for the default HIRES processing with a limit of twenty iterations.

($J = 2 \rightarrow 1$). L1246−SMM1 is known to be a protostar, but an outflow had not yet been detected. The ^{12}CO ($J = 2 \rightarrow 1$) line was detected in all cores, but no indication of high velocity gas was found in the cores L55−SMM1, L328−SMM1, L951−SMM1, L951−SMM2, L1014−SMM1 and L1246−SMM2. These cores are therefore very likely to be starless. L944−SMM1 and L1246−SMM1 did exhibit high velocity line wings, and we therefore proceeded with mapping the outflows (see section 5.2). Thus of the 10 cores identified in the SCUBA maps, we classify 6 as starless cores, and 2 as outflow sources. The nature of the cores in L860 is not known.

5. Protostars L944 and L1246

Our sample of dark molecular clouds contains 2 protostars. L1246−SMM1 is a previously known protostar and associated with IRAS 23228+4320, L944−SMM1 is a new discovery and not associated with an IRAS source. In the literature L1246−SMM1 is known as L1246, but in this paper that name is reserved for the cloud. The detection of L944−SMM1 demonstrates that IRAS based samples of young stellar objects are incomplete, and biased towards the more evolved (infrared) protostars. In the next sections the spectral energy distributions and outflows of both protostars are discussed.

5.1. Spectral energy distributions

Protostars are classified by the shapes of their spectral energy distributions. The classification of the infrared protostars depends upon the value of the infrared spectral index ($\alpha = -d\log(\nu F_\nu)/d\log(\nu)$) evaluated longward of 2.2 μm (Lada & Wilking 1984; Lada 1991). Class I and Class II objects both have a SED broader than that of a single-temperature blackbody, with $\alpha > 0$ and $\alpha \sim 0$ respectively. Class III sources have a SED with $\alpha < 0$, and the SED width is close to that of a single-temperature blackbody. The SED of a Class 0 source is also relatively narrow and corresponds to a blackbody temperature below 30 K (André et al. 1993).

The spectral energy distributions of the outflow driving sources in L944 and L1246 are derived using the SCUBA maps. We measure the flux densities at 450 and 850 μm in a 50$''$ aperture after having subtracted background emission. The L1246−SMM1 far infrared flux densities are from the IRAS point source catalogue. L944−SMM1 is not associated with an IRAS source, but the infrared flux densities for this source were obtained from HIRES data. Continuum emission at both 100 and 60 μm can be associated with L944−SMM1, and flux densities are measured in 240$''$ apertures after the subtraction of a background level. The spectral energy distributions have been fitted with a single temperature grey body spectrum (assuming the dust is optically thin) with β = 1.5, a value deviating from what was used to calculate the masses in the clouds, but suitable for the dust around protostars (Visser et al. 1998). The temperatures obtained from fitting the 850, 450 and 100-μm datapoints are 21 K and 19 K for L944−SMM1 and L1246−SMM1 respectively. The same temperature has been found by Launhardt et al. (1997) for L1246−SMM1. The spectral energy distribution of L944−SMM1 is fitted well by a single temperature greybody curve (T = 21 K, Figure 2), suggesting that this source is a Class 0 protostar. However, NIR observations are needed to rule out the possibility that this source is a Class I object.

Another feature of Class 0 sources is that the ratio L_{bol}/L_{submm} lies well below 200 (André et al. 1993). L_{bol} is the object's total luminosity, and L_{submm} is the luminosity radiated by the object at wavelengths longward of 350 μm. L_{submm} has been calculated by integrating under the greybody fits of Figure 2; L_{submm} for L944−SMM1 is 0.17 $L_{\odot}$, and for L1246−SMM1 0.3 $L_{\odot}$. We calculated L_{bol} between 1 and 1300 μm by assuming for L944−SMM1 that this source will not be detected in the NIR, and for L1246−SMM1 that a maximum luminosity of 20% will be radiated away in the NIR (between 1 to 12 μm). We obtain for L944−SMM1 a ratio of 4.4/0.2 = 22 and for L1246−SMM1 a ratio of (8.0 + 20%)/0.3 = 32. Launhardt et al. (1997) obtained a value L_{bol}/L_{submm} = 34 for L1246−SMM1 using NIR photometry, and concluded that the protostar in L1246 is a candidate Class 0 protostar (depending on the presence of an outflow). The L_{bol}/L_{submm} ratios for both L944−SMM1 and L1246−SMM1 are comfortably below 200, suggesting that if the assumptions are valid, both sources are Class 0 protostars.

5.2. Outflows

In Figure 3 we present the outflows in ^{12}CO ($J = 2 \rightarrow 1$) of the protostar in L944 and L1246 as observed with the JCMT. The total width of the outflow in L1246 at one sigma noise level is 6 km/s. The extent of the outflow is 0.28 pc, and the dynamical age of the outflow in L1246 is $\tau_{\rm d}$ = 0.28 pc/6 km s^{-1} = 4.6 $\times 10^{4}$ years. The dynamical age of the outflow in L944 is $\tau_{\rm d}$ = 0.37 pc/11 km s^{-1} = 3.3 $\times 10^{4}$ years (in both cases no correction has been made for a flow inclination). The total gas masses of the flows have been calculated assuming that the CO emission is optically thin, the number abundance of CO relative to H_2 is 5×10^{-5}, and the J levels were occupied in local thermodynamic equilibrium at a kinetic temperature of 20 K (similar to the dust temperature). The mass of blueshifted gas in the L944 outflow is $\sim$0.054 $M_\odot$, 10 times more massive than the redshifted outflow. The combined momentum and energy values of the outflowing gas are 0.19 $M_\odot$ km s^{-1} and 6.4 $\times 10^{35}$ J. In L1246 the redshifted outflow is the more massive one. Its mass is 0.015 $M_\odot$, compared with 0.004 $M_\odot$ of blueshifted gas. The combined momentum and energy of this outflow are 0.03 $M_\odot$ km s^{-1} and 0.59 $\times 10^{35}$ J. No corrections have been made for optical depth or inclination.

Class 0 sources are thought to drive more powerful outflows than Class I sources. This decrease of outflow energetics during the first evolutionary stages of a protostar probably reflects a corresponding decay in the mass accretion rate (Bontemps et al. 1996). The force (or momentum flux) of an outflow can be calculated by dividing the outflow momentum by the dynamical age of the outflow. To be able to compare the outflow forces of the protostars in L944 and L1246 with other outflows we have to correct for the optical depth of the CO emission and a possible inclination angle of the outflow. We use the same combined correction factor (i.e. 10) as applied by Bontemps et al. (1996). The momentum flux obtained is 5.7×10^{-5} $M_\odot$ km s^{-1} yr^{-1}, for the outflow in L944, and 7.2×10^{-6} $M_\odot$ km s^{-1} yr^{-1}, for the outflow in L1246. The outflow in L944 is thus a factor 10 more powerful than the outflow in L1246. The circumstellar envelope mass for the protostars are estimated to be 0.9 $M_\odot$ and 2.2 $M_\odot$ for L944−SMM1 and L1246−SMM1 respectively. These masses have been calculated from the flux density at 850 μm in a 50$''$ aperture after having subtracted background emission, and assuming $T_{dust} \sim 20$ K, and $\beta = 1.5$. The outflow efficiency is the outflow force divided by the radiative momentum flux (L_{bol}/c) and equals $\sim$630 for L944−SMM1, and $\sim$40 for L1246−SMM1. We can now place the two protostars on the efficiency versus $M_{env}/L_{bol}^{0.6}$ diagram (see Figure 7, Bontemps et al. 1996) using these numbers together with the estimated bolometric luminosity in the previous section. Both protostars lie in the region occupied by Class 0 sources, although the outflow efficiency of L1246−SMM1 is somewhat lower than that of the other Class 0 sources in Figure 7 of Bontemps et al. Note, however, that this source has been classified as a Class 0 source by Launhardt et al. (1997) based on NIR photometry. It is possible that the distance towards this source is not as much as 730 pc, and the outflow might thus be more efficient since the outflow efficiency scales as 1/D.

6. Implications for star formation

All the clouds in this sample are compact and most are Bok globules. Bok globules are small, round, dense nebulae that are known to be sites of star formation (Bok & Reilly, 1947). However, some of the clouds are not very symmetrical and their morphologies indicate that the material has been swept up by a shock or wind, i.e. they have a sharp edge on one side and are fuzzy on the other side (L860, L951, L1103). The two protostars are detected in Bok globules, but both the round globules and the more irregular shaped clouds seem to be forming high density cores which might be prestellar cores on their way to become protostars. Overall though, the clouds are very quiescent and only 7 of them seem to be actively forming stars at the present time. So although Bok globules are known to be sites of star formation, not all Bok globules form stars at the present time.

In ρ Ophiuchus the ratio of Class 0 sources to Class I sources is approximately 1:10 (André & Montmerle 1994), very different from what we find in these rather isolated compact dark molecular clouds. We identified 2 Class 0 objects and *no* Class I objects. This could suggest that the duration of the different protostellar phases might be different in our sample in comparison with ρ Ophiuchus possibly due to different initial conditions. Alternatively, it could mean that the survey in ρ Ophiuchus samples a star burst event which occurred few $\times 10^5$ yr ago, explaining the large number of Class I objects compared with the number of Class 0 objects. In any case this result seems to suggest that star formation is environment dependent although the size of our sample makes this conclusion tentative. A more extended search for protostars in a larger sample of dark molecular clouds is needed to confirm this. Also, $2\,\mu$m observations are needed to ascertain the classification of the protostars.

7. Conclusions

For the first time an imaging survey of optically dark molecular clouds has been carried out at a submillimetre wavelength ($850\,\mu$m). The sample comprises 24 compact Lynds clouds, and constitutes the first part of a more extended survey. The clouds selected are the most opaque ones from the Lynds catalogue, and the optical selections assures the sample is unbiased towards infrared properties. Of the 24 clouds, 19 have been detected, and the dust emission follows the optical extinction very well. The undetected clouds are either a few degrees colder and/or have a column density below our detection limit. A total of 10 submillimetre cores have been identified in just 7 clouds, and the clouds are thus in general quiescent. Two of the cores (L944−SMM1 and L1246−SMM1) contain protostars which drive outflows. L1246−SMM1 is a known protostar associated with IRAS 23228+4320, and protostar L944−SMM1 is a new discovery not associated with an IRAS source. The detection of L944−SMM1 emphasizes the importance of the optical selection of the dark clouds. The outflows of both protostars are new detections and confirm the protostellar status for both sources. The outflow from the protostar in L944 is more massive, more powerful, and more efficient than the outflow of the protostar in L1246. The outflow in L1246 is still consistent with a Class 0 source. Although numbers are limited in this sample it is remarkable that the two protostars found seem to be Class 0 sources, while the lifetime of this youngest protostellar phase from observations of large star formation complexes such as ρ Ophiuchus is believed to be ten times shorter than the lifetime of the more evolved Class I phase.

This might indicate that the initial conditions of star formation vary with environment, or that star formation is triggered by some external factor, resulting in localized star bursts. The 8 remaining submillimetre cores are candidate pre-stellar cores, but their nature and dynamics needs to be further studied using molecular line observations.

Acknowledgments

The authors wish to thank the referee A. Gibb for his useful comments which helped to clarify the text. We would also like to thank Iain Coulson for observing some of the cores in ^{12}CO. The James Clerk Maxwell Telescope is operated by the Joint Astronomy Centre on behalf of the Particle Physics and Astronomy Research Council of the United Kingdom, the Netherlands Organisation for Scientific Research, and the National Research Council of Canada. AEV was supported by a Marie Curie Research Training Grant, JSR and CJC acknowledge the support of a Royal Society Fellowship and a PPARC Advanced Fellowship respectively.

REFERENCES

André, P., Montmerle, T., 1994, ApJ, 420, 837

André, P., Ward-Thompson, D., Barsony, M., 1993, ApJ, 406, 122

André, P., Ward-Thompson, D., Barsony, M., 1999, in Protostars and Planets IV, ed. V. Mannings, A. P. Boss & S. S. Russell (Tucson: University of Arizona Press), in press

André, P., Ward-Thompson, D., Motte, F., 1996, A&A, 314, 625

Aumann, H.H., Fowler, J.W., Melnyk, M., 1990, AJ, 99, 1674

Bacmann, A., André, P., Puget, J.L., Abergel, A., Bontemps, S., Ward-Thompson, D., 2000, accepted in A&A

Barnard, E.E., 1927, "Atlas of Selected Regions of the Milky Way", edt. Frost, E.B., Calvert, M.R., Carnegie Institute of Washington

Basu, S., Mouschovias, T.Ch., 1994, ApJ, 432, 720

Bernard, J.P. et al. 1999, A&A, 347, 640

Bohlin, R.C., Savage, B.D., Drake, J.F., 1978, ApJ, 224, 132

Bok, B.J., Reilly, E.F., 1947, ApJ, 105, 255

Bontemps, S., André, P., Terebey, S., Cabrit, S., 1996, A&A, 311, 858

Chen, H., Myers, P.C., Ladd, E.F., Wood, D.O.S., 1995, ApJ, 445, 377

Ciolek, G.E., Mouschovias, T.Ch., 1994, ApJ, 425, 142

Clemens, D.P., Barvainis, R., 1988, ApJS, 68, 257

Clemens, D.P., Yun, J.L., Heyer, M.H., 1991, ApJS, 75, 877

Cohen, M., Kuhi, L.V., 1979, ApJSS, 41, 743

Dame, T.M., Thaddeus, P., 1985, ApJ, 297, 751

Dame, T.M., Ungerechts, H., Cohen, R.S., De Geus, E.J., Grenier, I.A., May, J., Murphy, D.C., Nyman, L.A., Thaddeus, P., 1987, ApJ, 322, 706

Dobashi, K., Bernard, J-P., Yonekura, Y., Fukui, Y., 1994, ApJS, 95, 419

Emerson, J.P., 1987, Star Forming Regions, IAU Symp. No. 115, eds. Peimbert, M., Jugaku, J., Reidel, Dordrecht, Holland

Foster, P.N., Cevalier, R.A., 1993, ApJ, 416, 303

Gomez, M., Kenyon, S.J., Hartmann, L., 1994, 107, 1850

Henning, Th., Michel, B., Stognienko, R., 1995, Plant. Space Sci., 43, 1333

Henriksen, R., André, P., Bontemps, S., 1997, A&A, 323, 549

Hildebrand, R.H., 1983, QJRAS, 24, 267

Hilton, J., Lahulla, J.F., 1995, A&AS, 113, 325

Holland, W.S., Cunningham, C.R., Gear, W.K., Jenness, T., Laidlaw, K., Lightfoot, J.F., Robson, E.I., 1998, Proceeding of the International Society for Optical Engineering, 3357, 305

Huard, T.L., Sandell, G., Weintraub, D.A., 1999, ApJ, accepted

Jenness, T., Lightfoot, J.F., 1998, Starlink User Note 216, Starlink Project, CLRC

Kenyon, S.J., Hartmann, L.W., 1990, ApJ, 349, 197

Kenyon, S.J., Hartmann, L.W., Strom, K.M., Strom, S.E., 1990, AJ, 99, 869

Königl, A., Pudritz, R.E., 1999, in Protostars and Planets IV, ed. V. Mannings, A. P. Boss & S. S. Russell (Tucson: University of Arizona Press), in press

Lada, C.J., Wilking, B.A., 1984, ApJ, 287, 610

Lada, C.J., 1991, in the Physics of Star Formation and Early Stellar Evolution, C.J. Lada & N.D., Kylafis, Dordrecht; Reidel, 329

Launhardt, R., Henning, Th., 1997, A&A, 326, 329, (L&H)

Launhardt, R., Ward-Thompson, D. Henning, Th., 1997, MNRAS, 288, 45L

Lee, C.W., Myers, C., 1999, submitted

Leung, C.M., Kutner, L., Mead, K.N., 1982, ApJ, 262, 583

Lynds, B.T., 1962, ApJS, 7, 1

McLaughlin, D.E., Pudritz, R.E., 1997, ApJ, 476, 750

Motte, F., André, P., Neri, R., 1998, A&A, 336, 150

Myers, P.C., Benson, P.J. 1983, ApJ, 266, 309

Nozawa, S., Mizuno, A., Teshima, Y., Ogawa, H, Fukui, Y., 1991, ApJS, 77, 647

Parker, N.D., 1988, MNRAS, 235, 139

Robert, C., Pagani, L., 1993, A&A, 271, 282

Shu, F.H., 1977, ApJ, 214, 488

Visser, A.E., Richer, J.S., Chandler, C.J., Padman, R., 1998, MNRAS, 301, 585

Ward-Thompson, D., Scott, P.F., Hills, R.E., André, P., 1994, MNRAS, 268, 276

Wilking, B.A., Lada, C.J., Young, E.T., 1989, ApJ, 340, 823

Williams, J.P., Myers, P.C., Wilner, D.J., Di Francesco, J., 1999, ApJ, 513, L61

Yonekura, Y., Dobashi, K., Mizuno, A., Ogawa, H., Fukui, Y., 1997, ApJS, 110, 21

Table 1. Positions[a], LSR velocities, distances, references, other names, and associated cloud complexes.

Source	R.A. (1950) (h m s)	Dec. (1950) (° ′ ″)	v_{lsr} km/s	D pc	References[b]	Other Names	Associated Complex
L31	16 47 31	−19 02 15	4.8	160	I	CB67	Ophiuchus
L53	17 20 26	−23 59 45		160			Ophiuchus
L55	17 19 55	−23 54 30	4.6	160		B69	Ophiuchus
L222	17 38 24	−19 46 00	10.6	160		CB94	Ophiuchus
L223	17 37 53	−19 42 00	10.3	160		CB93	Ophiuchus
L226	17 37 45	−19 38 00	10.5	160	I	CB92	Ophiuchus
L229	17 37 26	−19 31 15		160			Ophiuchus
L231	17 37 31	−19 32 45		160			Ophiuchus
L233	17 42 18	−20 00 00	11.1	160	I	B83A, CB95	Ophiuchus
L328	18 14 05	−18 03 00	6.6	190	I, II	B93, CB131	
L675	19 21 31	+11 01 45	7.5	300	VIII	CB193	Cloud B
L709	19 11 39	+16 21 45	6.3	300	I	CB184	Cloud B
L860	20 01 26	+35 53 15		700	III	B146	Cygnus Rift
L917	20 38 11	+43 58 00		700	III		Cygnus Rift
L944	21 15 48	+43 05 30	5.0	700	III		Cygnus Rift
L951	21 18 20	+43 18 45	5.2	700	III		Cygnus Rift
L953	21 19 32	+43 08 15	6.3	700	III		Cygnus Rift
L1014	21 22 18	+49 46 30	4.7	200	IV, V		
L1021	21 19 58	+50 44 30		200	II		
L1103	21 40 34	+56 30 00		150			
L1111	21 38 54	+57 34 30	-0.9	150	V	B161, CB233	
L1166	22 03 47	+59 19 00	-2.9	300	VII	B173, CB236	
L1185	22 27 34	+58 54 00		300	VI		
L1246	23 23 00	+63 20 00	-11.1	730	VI	CB243	Cepheus OB3 complex

[a]Positions of clouds adopted from Parker (1988)

[b](I) Launhardt & Henning 1997; (II) Lee & Myers 1999; (III) Dame & Thaddeus 1985; (IV) Robert & Pagani 1993; (V) Leung et al. 1982; (VI) Yonekura et al. 1997; (VII) Dobashi et al. 1994; (VIII) Dame et al. 1987

Table 2. IRAS PSC associations, peak fluxes, integrated fluxes of the clouds, and noise levels (on each 3″ pixels).

Source	IRAS association	Peak F_ν		Integrated F_ν		Noise	
		450 μm	850 μm	450 μm	850 μm	450 μm	850 μm
		mJy/beam	mJy/beam	Jy	Jy	mJy/beam	mJy/beam
L31	16482−1906		106		4.6		23
L53	17205−2359		<111				37
L55			101		1.1		15
L222			115		0.3		22
L223			115		0.4		24
L226	17375−1936		<96				32
L229			<84				28
L231			<78				26
L233			<69				23
L328		700	211	8.0	1.7	120	15
L675			67		0.1		18
L709	19116+1623		59		0.6		12
L860			93		1.0		13
L917			91		1.1		19
L944		810	214	4.7	1.4	120	15
L951	21186+4320		71		0.5		22
L953			63		0.2		17
L1014		800	146	5.3	0.9	120	15
L1021			93		0.7		25
L1103			108		1.4		28
L1111			96		0.7		26
L1166			102		0.7		20
L1185			90		0.9		24
L1246	23228+6320	1850	402	13.1	4.0	150	17

Table 3. The peak mass and corresponding column density, space density[a] and A_v, total mass and corresponding column density.

Source	Peak Mass $M_\odot$	Peak $N(H_2)$ m^{-2}	Peak $n(H_2)$ m^{-3}	Peak A_v mag	Total Mass $M_\odot$	Averaged $N(H_2)$ m^{-2}
L31	0.06	1.5×10^{26}	3.9×10^{11}	15	2.2	5.5×10^{25}
L53	<0.05	$<1.5\times10^{26}$	$<4.0\times10^{11}$	<16		
L55	0.05	1.3×10^{26}	3.6×10^{11}	14	0.5	4.7×10^{25}
L222	0.06	1.5×10^{26}	4.1×10^{11}	16	0.2	5.5×10^{25}
L223	0.06	1.5×10^{26}	4.1×10^{11}	16	0.2	5.8×10^{25}
L226	<0.05	$<1.3\times10^{26}$	$<3.5\times10^{11}$	<13		
L229	<0.04	$<1.1\times10^{26}$	$<3.0\times10^{11}$	<12		
L231	<0.04	$<1.0\times10^{26}$	$<2.8\times10^{11}$	<11		
L233	<0.03	$<0.9\times10^{26}$	$<2.5\times10^{11}$	<10		
L328	0.14	2.8×10^{26}	6.4×10^{11}	30	1.2	10.8×10^{25}
L675	0.11	0.9×10^{26}	1.3×10^{11}	9	0.2	3.4×10^{25}
L709	0.10	0.8×10^{26}	1.1×10^{11}	8	1.0	3.1×10^{25}
L860	0.87	1.2×10^{26}	0.8×10^{11}	13	9.4	3.6×10^{25}
L917	0.85	1.2×10^{26}	0.7×10^{11}	13	10.4	4.4×10^{25}
L944	1.99	2.9×10^{26}	1.8×10^{11}	30	13.0	6.0×10^{25}
L951	0.66	0.9×10^{26}	0.6×10^{11}	10	4.7	4.0×10^{25}
L953	0.59	0.8×10^{26}	0.5×10^{11}	9	2.2	3.6×10^{25}
L1014	0.11	1.9×10^{26}	4.2×10^{11}	20	0.7	6.0×10^{25}
L1021	0.07	1.2×10^{26}	2.7×10^{11}	13	0.5	4.8×10^{25}
L1103	0.05	1.4×10^{26}	4.1×10^{11}	15	0.6	5.6×10^{25}
L1111	0.04	1.3×10^{26}	3.7×10^{11}	13	0.3	5.0×10^{25}
L1166	0.17	1.4×10^{26}	2.0×10^{11}	14	1.2	4.9×10^{25}
L1185	0.15	1.2×10^{26}	1.7×10^{11}	13	1.5	4.5×10^{25}
L1246	4.07	5.4×10^{26}	3.2×10^{11}	56	40.1	8.9×10^{25}

[a]The space densities are calculated assuming the depth of the cloud is one beamsize, and are therefore upper limits.

Table 4. Positions and peak flux densities at 850 μm of the 10 submillimetre cores identified in the maps. Also indicated was whether or an outflow has been detected.

Source	R.A.(1950) (h m s)	Dec.(1950) (° ′ ″)	Peak $F_{850\mu m}$ mJy/beam	outflow detected
L55−SMM1	17 19 55.3	−23 55 30	101	no
L328−SMM1	18 14 05.0	−18 03 12	211	no
L860−SMM1	20 01 25.9	+35 53 30	93	
L860−SMM2	20 01 29.0	+35 52 57	83	
L944−SMM1	21 15 51.2	+43 06 08	214	yes
L951−SMM1	21 18 20.0	+43 19 17	71	no
L951−SMM2	21 18 22.9	+43 19 51	67	no
L1014−SMM1	21 22 23.9	+49 46 06	146	no
L1246−SMM1	23 22 51.9	+63 20 10	402	yes
L1246−SMM2	23 23 03.5	+63 20 16	174	no

Appendix: Distances

To be able to obtain physical parameters from the data the correct distances towards the clouds need to be known. It is difficult to obtain distances because both star counts and kinematic determinations cannot be used efficiently for these small and nearby ($D < 1$ kpc) clouds. A method often applied is to associate the dark clouds with larger molecular cloud complexes, assuming the small clouds are not as isolated as it might seem, see for instance Launhardt & Henning (1997 hereafter L&H). We used this method to obtain the distances towards some of our clouds (see next paragraph) and compared these with values in the literature (Hilton & Lahulla 1995). In Table 1 we list the LSR velocities, distances and associated complexes where appropriate. Also in Table 1 are names for the clouds from the Barnard (B) catalogue (1927) and the Clemens and Barvainis (CB) catalogue (1988). The LSR velocity is from Clemens et al (1991) if the cloud is associated with a cloud from the Clemens and Barvainis catalogue. The LSR velocities of L55, L944, L953 and L1014 come from our ^{12}CO observations.

A well known star forming region is ρ Ophiuchus of which the boundaries and velocity are given by Dame et al. (1987). Within these boundaries and with similar LSR velocities are the clouds L31, L53 and L55 (Nozawa et al. 1991). Also associated with Ophiuchus is L226 (L&H), but the velocity of this cloud is 10.5 km/s, different from the 3 km/s thought to be the LSR velocity of Ophiuchus. Clouds L222, L223, L229, L231 are very near to L226, and they seem to form a small cluster presumably all at the same distance. Another nearby cloud with similar velocity as L226 is L233. The distance towards ρ Ophiuchus is 160 pc (Chen et al. 1995), which is the distance we adopt for the clouds associated with this region.

Cloud L328 is thought to be at a distance of 180 pc according to L&H and at a distance of 200 pc according to Lee & Myers (1999). The distance adopted here is 190 pc. Both L675 and L709 are thought to be part of Cloud B towards the distance is 300 pc (L&H).

We have associated both L860 and L917 with the Cygnus Rift which has a distance of 700 pc, and LSR velocity 7 km/s (Dame et al. 1987). Dobashi et al. (1994) associated L917 with the

Cygnus X complex which is at a distance of 1700 pc (v_{lsr}=2 km/s). A velocity measurement of L917 is needed to determine which association is more likely. The three other clouds we have associated with the Cygnus Rift are very near to this molecular cloud complex, but although they have similar velocities, they are not directly in it. It is however the nearest complex with which these rather isolated clouds could be associated.

L1014 has been linked to B362 by Robert & Pagani (1993) for which the distance is thought to be 200 pc (Leung et al. 1982). A cloud nearby L1014 is L1021, which might be at the same 200 pc distance (Lee & Myers 1999). However Dobashi et al. (1994) associate L1014 with ^{13}CO cloud D83, and L1021 with ^{13}CO cloud D98, both associated with Cygnus OB7 at a distance of 800 pc, LSR velocity -1 km/s (Dame & Thaddeus 1985). The distance towards L1103 and L1111 is thought to be 150 pc (Leung et al. 1982; Lee & Myers 1999). But again, according to Dobashi et al. (1994) L1111 is associated with ^{13}CO cloud D138, which has a distance of 750 pc. L1166 is near L1165 towards which the distance is 300 pc (Dobashi et al. 1994). The distance towards L1185 comes from the association with ^{13}CO cloud Y20 in cloud group 3 (Yonekura et al. 1997). And finally, L1246 has been associated with the Cepheus OB3 complex at a distance of 730 pc.

We conclude that the distances presented here and used throughout this work might not be entirely reliable. Mainly the distances towards the "L226 cluster" and L944, L951, L953 are uncertain, and the distances towards L917, L1014, L1021, L1103 and L1111 might be underestimated.

Figure captions

Fig. 1a. Images of four compact cores. The greyscale is from the STScI Digitized Sky Survey and is overlaid with the continuum contours. *Left* the 450-μm continuum contours and *right* the 850-μm continuum contours. All submillimetre maps are smoothed with a 14$''$ gaussian. The 450-μm contour levels are the following: L328: 2σ, 3σ, 4σ; L944: 2σ, 3σ, 4σ, 5σ, 6σ, 7σ; L1014: 2σ, 4σ, 6σ, 8σ, 10σ; L1246: 2σ, 4σ, 6σ, 8σ, 10σ, 12σ.

The 850-μm contour levels are as follows: L328: 3σ, 4σ, 5σ, 6σ, 7σ; L944: 1σ, 2σ, 3σ, 4σ, 5σ, 6σ, 7σ; L1014: 1σ, 2σ, 3σ, 4σ, 5σ, 6σ; L1246: 3σ, 6σ, 9σ, 12σ, 15σ, 18σ, 21σ, 24σ, 27σ. The noise levels on the smoothed images gives σ.

Fig. 1b. Images of the remaining detected Lynds clouds. The greyscale is from the Digitized Sky Survey and is overlaid with the 850-μm continuum contours. All the submillimetre maps are smoothed with a 14$''$ gaussian apart from L31, and L1103 which have been smoothed with a 24$''$ gaussian, and L1021, L111, and L1185 which have been smoothed with a 20$''$ gaussian. The contour levels are as follows (with σ the noise levels on the smoothed images): L31: 1σ, 2σ, 3σ, 4σ, 5σ; L55: 1σ, 2σ, 3σ, 4σ; L222: 2σ, 4σ; L223: 3σ, 5σ; L675: 1σ, 2σ, 3σ; L709: 3σ, 5σ; L860: 2σ, 4σ, 6σ, 8σ, 10σ; L917: 2σ, 4σ; L951: 2σ, 3σ, 4σ, 5σ; L953: 2σ, 3σ, 4σ, 5σ; L1021: 2σ, 4σ; L1103: 2σ, 3σ, 4σ; L1111: 1σ, 2σ, 3σ; L1166: 3σ, 4σ, 5σ; L1185: 2σ, 4σ.

Fig. 2 The spectral energy distributions of the protostars in L944 and L1246.

Fig. 3 Outflow in L944: redshifted gas is integrated over the range 7.0 to 9.0 km/s (solid contours at $\int T_A^* \, dv = (0.4 + 0.2n)\,\mathrm{K\,km\,s^{-1}}$, for n=1-5) and the blueshifted gas is integrated over the range -2.0 to 3.0 km/s (dash dot contours at $\int T_A^* \, dv = (5 + 0.4n)\,\mathrm{K\,km\,s^{-1}}$, for n=1-6). Outflow in L1246: redshifted gas is integrated over the range -10.0 to -8.5 km/s (solid contours at $\int T_A^* \, dv = (1 + 0.5n)\,\mathrm{K\,km\,s^{-1}}$, for n=1-5) blueshifted gas is integrated from -13.5 km/s to -12.5 km/s (dash dot contours at $\int T_A^* \, dv = (0.35 + 0.2n)\,\mathrm{K\,km\,s^{-1}}$, for n=1-5). The outflows are overlaid on the SCUBA 850-μm images.

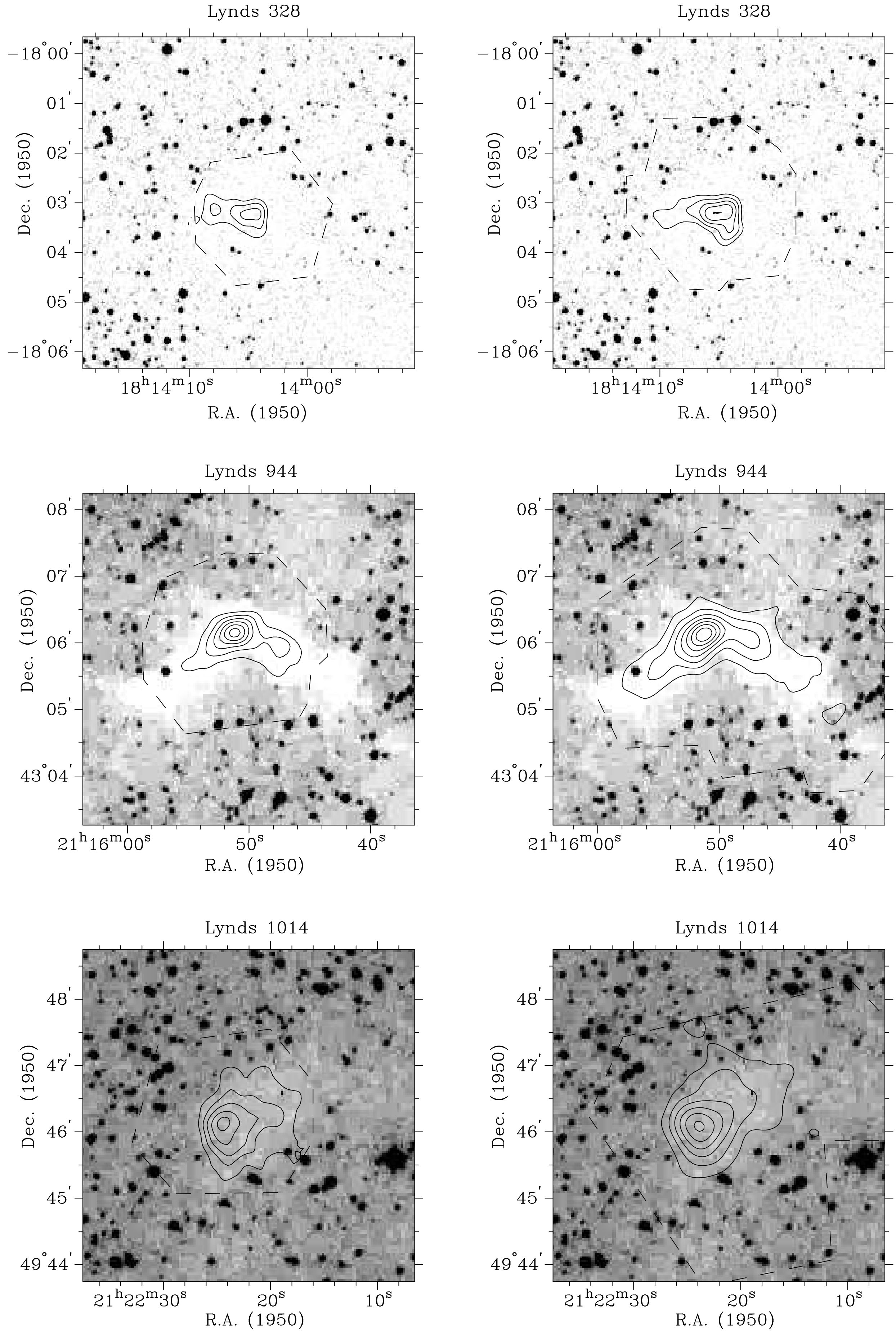
Lynds 328
Lynds 328
−18°00′
01′
02′
03′
04′
05′
−18°06′
Dec. (1950)
18h14m10s
14m00s
R.A. (1950)
Lynds 944
Lynds 944
08′
07′
06′
05′
43°04′
21h16m00s
50s
40s
Lynds 1014
Lynds 1014
48′
47′
46′
45′
49°44′
21h22m30s
20s
10s

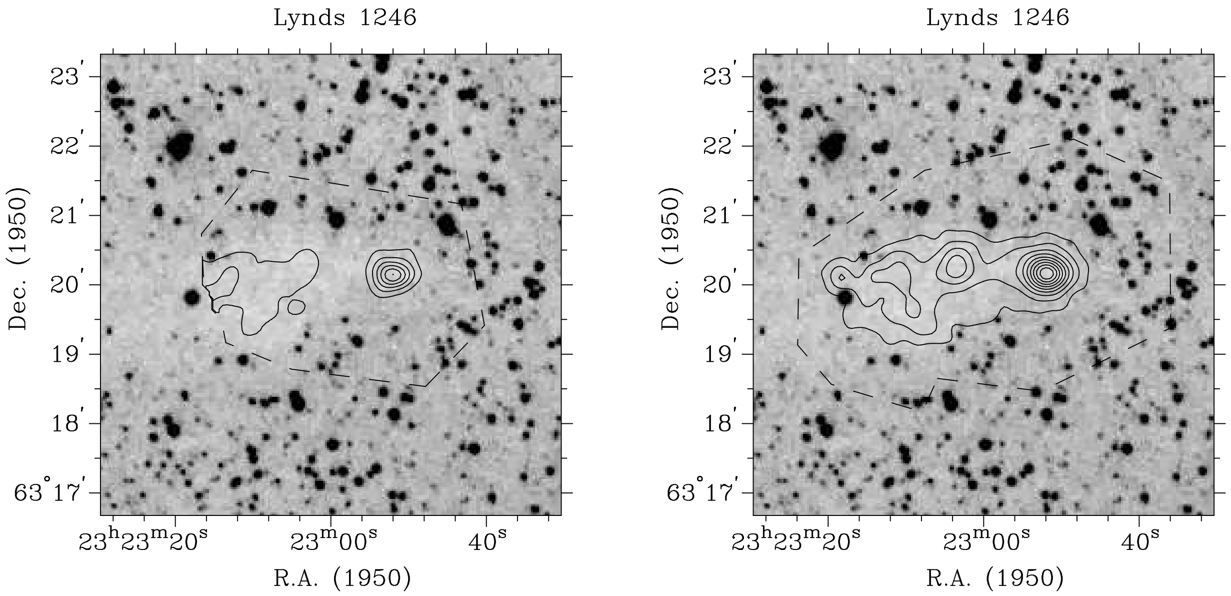
Lynds 1246
Dec. (1950)
23′
22′
21′
20′
19′
18′
63°17′
23h23m20s
23m00s
40s
R.A. (1950)
Lynds 1246
Dec. (1950)
23′
22′
21′
20′
19′
18′
63°17′
23h23m20s
23m00s
40s
R.A. (1950)

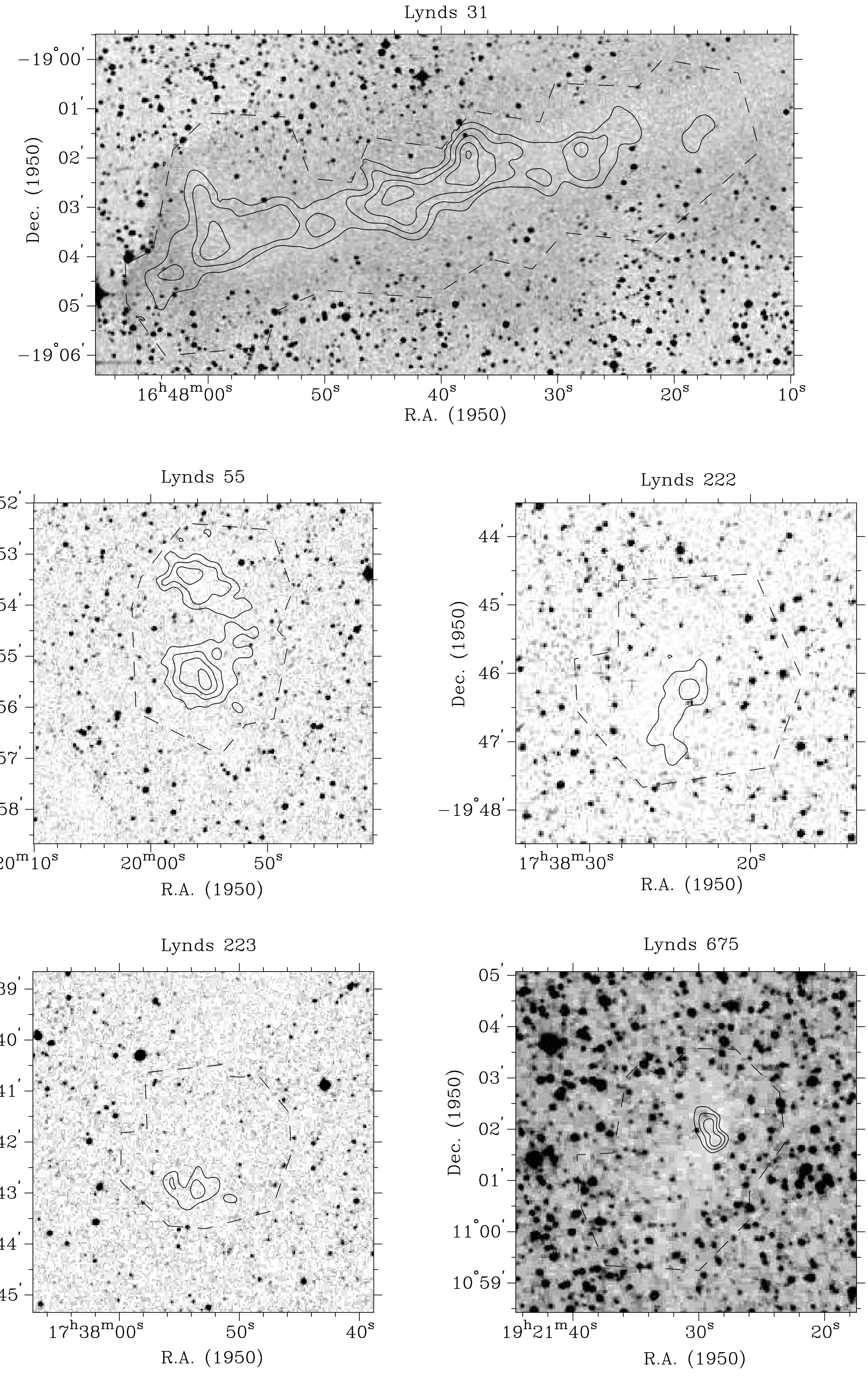
Lynds 31
Dec. (1950)
R.A. (1950)
−19°00′
01′
02′
03′
04′
05′
−19°06′
16h48m00s
50s
40s
30s
20s
10s
Lynds 55
Dec. (1950)
R.A. (1950)
52′
53′
54′
55′
56′
57′
−23°58′
17h20m10s
20m00s
50s
Lynds 222
Dec. (1950)
R.A. (1950)
44′
45′
46′
47′
−19°48′
17h38m30s
20s
Lynds 223
Dec. (1950)
R.A. (1950)
39′
40′
41′
42′
43′
44′
−19°45′
17h38m00s
50s
40s
Lynds 675
Dec. (1950)
R.A. (1950)
05′
04′
03′
02′
01′
11°00′
10°59′
19h21m40s
30s
20s

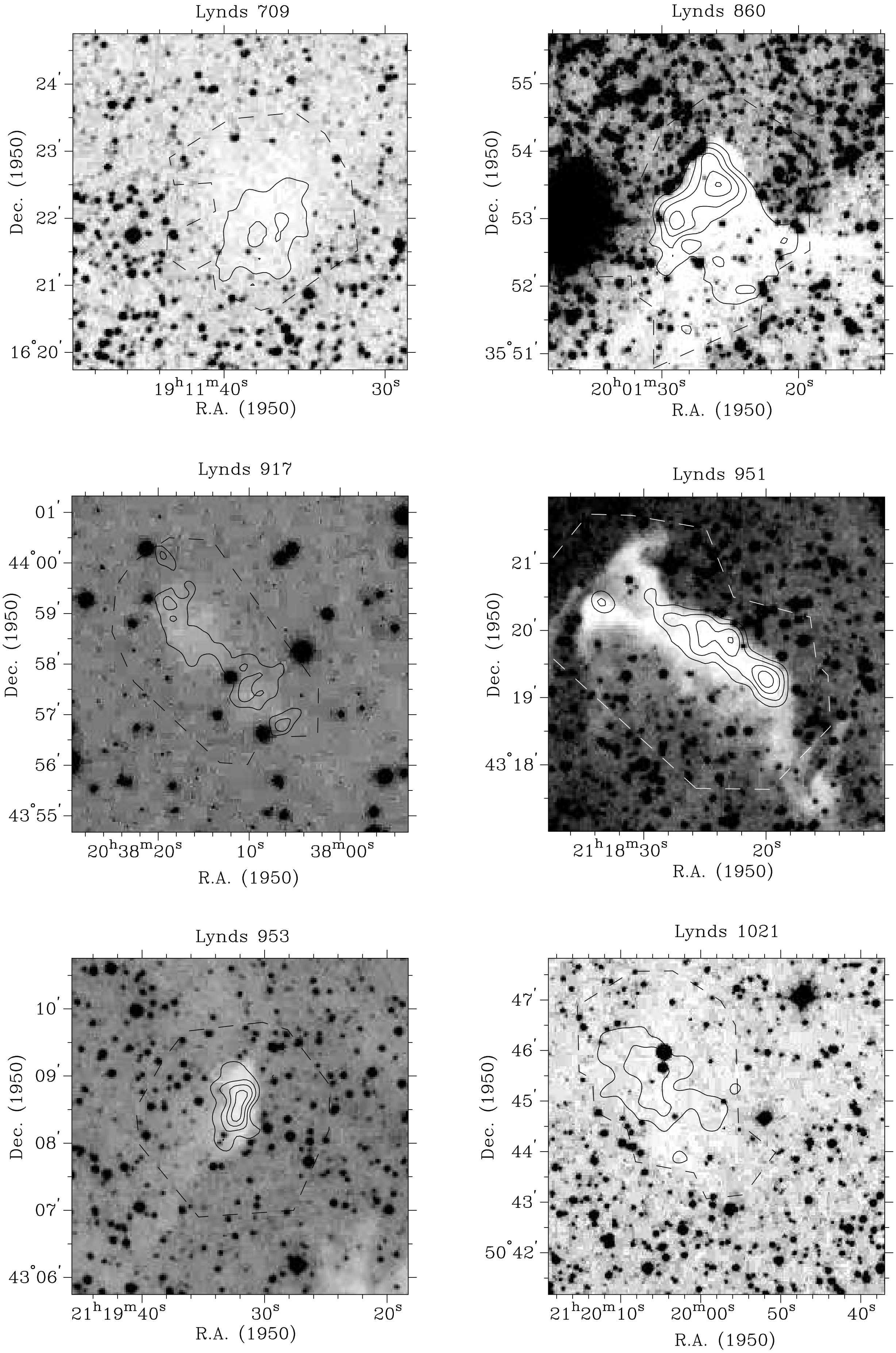
Lynds 709
24′
23′
22′
21′
16°20′
Dec. (1950)
19h11m40s
30s
R.A. (1950)
Lynds 860
55′
54′
53′
52′
35°51′
Dec. (1950)
20h01m30s
20s
R.A. (1950)
Lynds 917
01′
44°00′
59′
58′
57′
56′
43°55′
Dec. (1950)
20h38m20s
10s
38m00s
R.A. (1950)
Lynds 951
21′
20′
19′
43°18′
Dec. (1950)
21h18m30s
20s
R.A. (1950)
Lynds 953
10′
09′
08′
07′
43°06′
Dec. (1950)
21h19m40s
30s
20s
R.A. (1950)
Lynds 1021
47′
46′
45′
44′
43′
50°42′
Dec. (1950)
21h20m10s
20m00s
50s
40s
R.A. (1950)

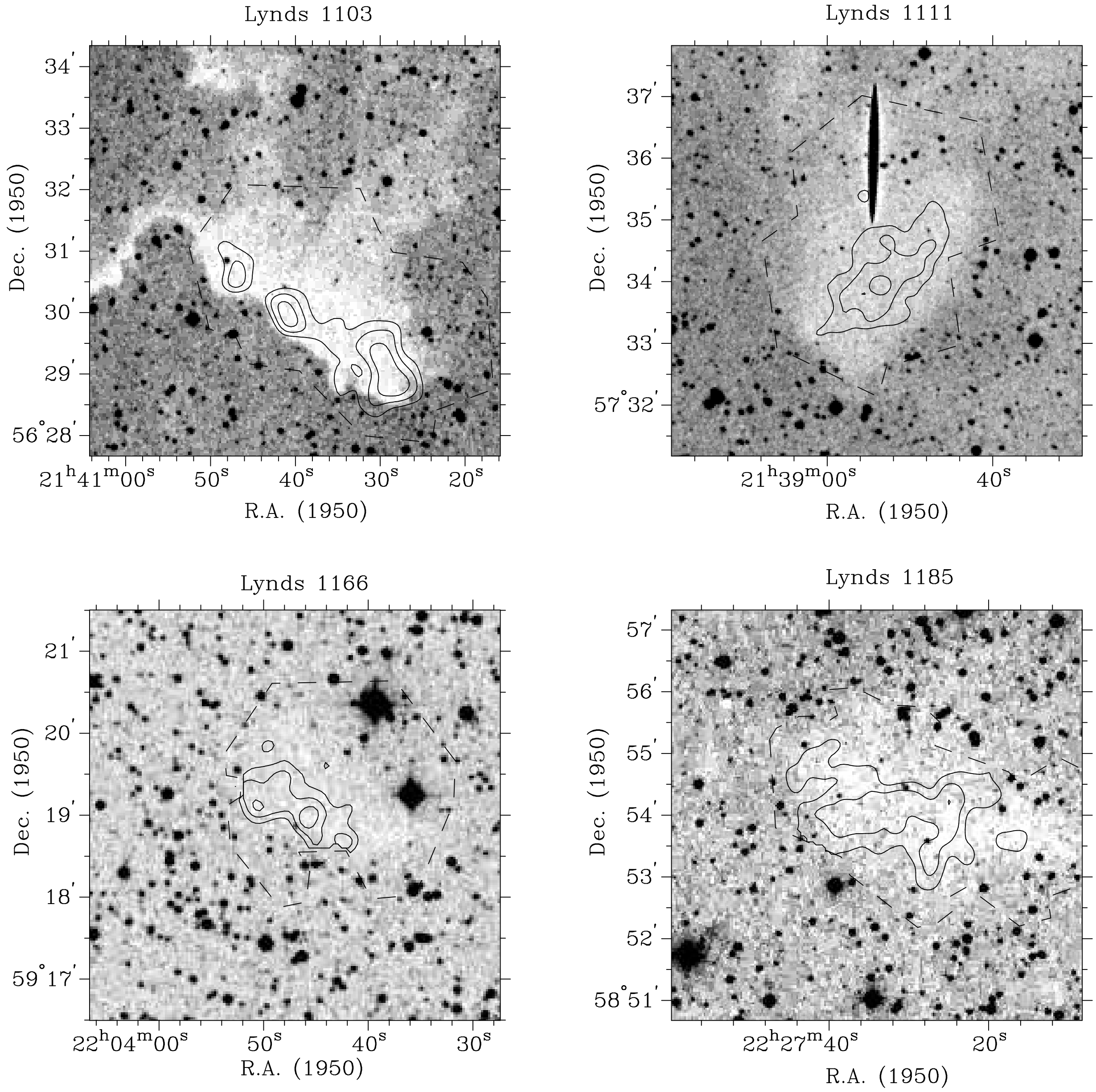
Lynds 1103
Dec. (1950)
34′
33′
32′
31′
30′
29′
56°28′
21h41m00s
50s
40s
30s
20s
R.A. (1950)
Lynds 1111
Dec. (1950)
37′
36′
35′
34′
33′
57°32′
21h39m00s
40s
R.A. (1950)
Lynds 1166
Dec. (1950)
21′
20′
19′
18′
59°17′
22h04m00s
50s
40s
30s
R.A. (1950)
Lynds 1185
Dec. (1950)
57′
56′
55′
54′
53′
52′
58°51′
22h27m40s
20s
R.A. (1950)

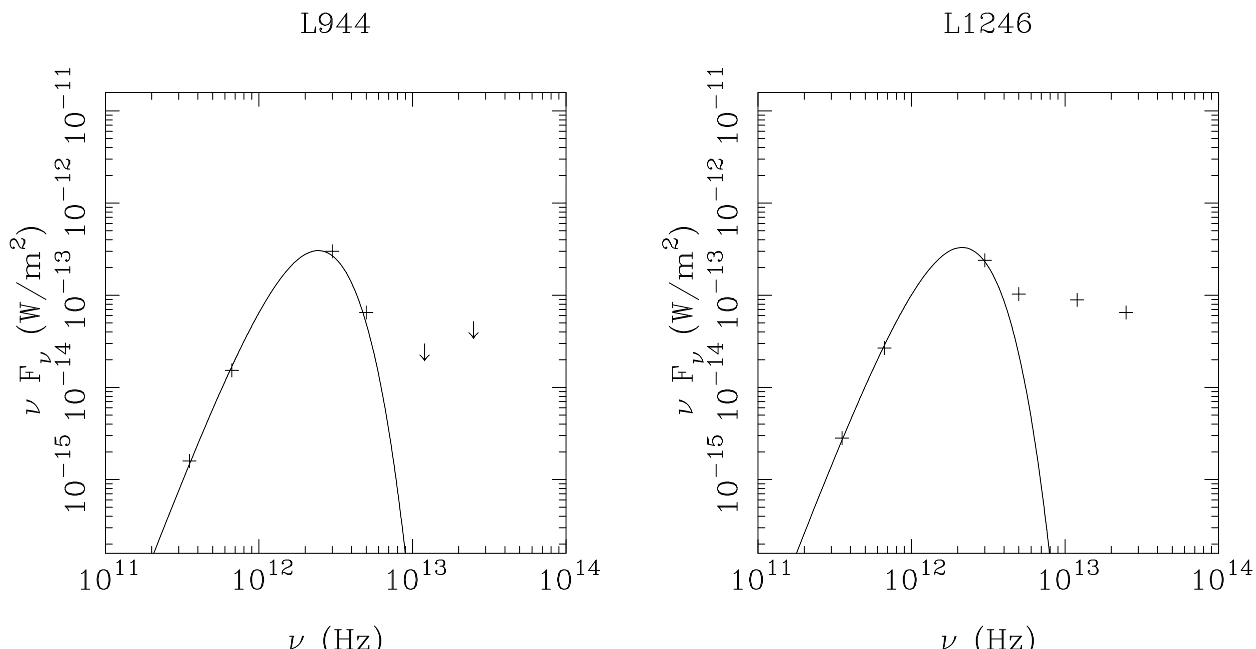
L944
L1246
ν F_ν (W/m^2)
10^{-15}
10^{-14}
10^{-13}
10^{-12}
10^{-11}
10^{11}
10^{12}
10^{13}
10^{14}
ν (Hz)

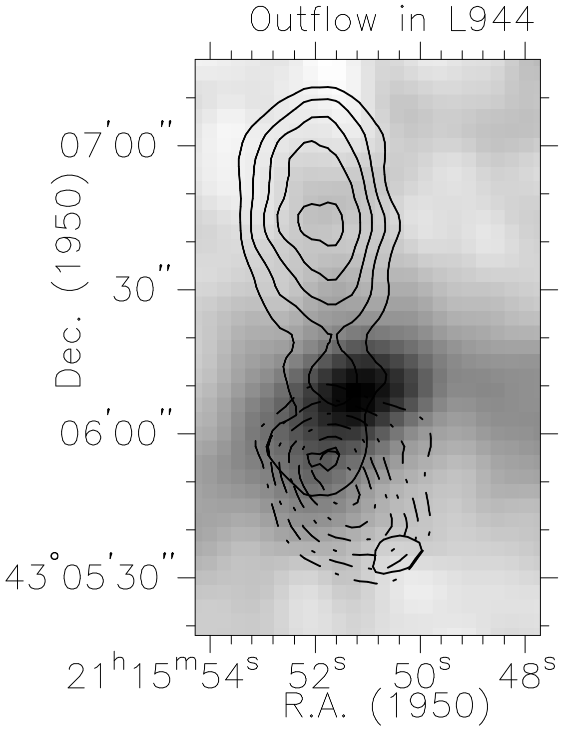
Outflow in L944
07'00"
30"
06'00"
43°05'30"
Dec. (1950)
21h15m54s
52s
50s
48s
R.A. (1950)

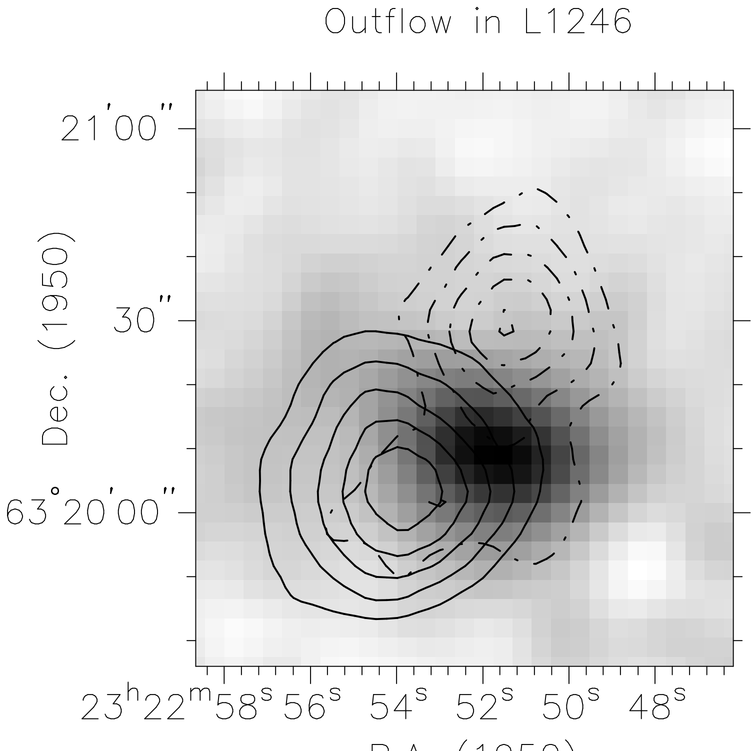
Outflow in L1246
21'00"
30"
63°20'00"
Dec. (1950)
23h22m58s
56s
54s
52s
50s
48s
R.A. (1950)